Flexible Over-the-Tube Device for Soft-Tethered Colonoscopy

Yu Huan, Xuyang Ren, Andrea Firrincieli, Luigi Manfredi, *Member, IEEE*, Matteo Cianchetti, *Member, IEEE*, Alberto Arezzo, Edoardo Sinibaldi, *Member, IEEE*, and Gastone Ciuti, *Senior Member, IEEE*

***Abstract*—Soft-tethered colonoscopes were proposed for safe and effective colon navigation, yet the deployment of front-wheel actuated colonoscopes is hindered by contact interactions with the lumen along the entire soft tether. To mitigate this problem, this study introduces an over-the-tube flexible device aimed to assist colonoscope deployment. The device is composed of three pneumatically driven actuators devised to repeatedly perform a two-phase operation: (phase I) to advance along the tether up to a working position relatively close to the colonoscope's tip; (phase II) to clamp and drag the tether forward, upon anchoring to the colonic wall. This way, a distal tether portion is freed, thus reducing the aforementioned limitations and fostering effective front-wheel navigation. Considering anatomical/clinical constraints and a 2N resistive force, we designed and prototyped a system with an inner and outer diameter of 12 and 26 mm, respectively, a length of 91 mm, and operating pressures equal to 150, 50, and 15 kPa for clamping the tether, elongating the device and safely anchoring to the colonic wall, respectively. The device was successfully tested, achieving locomotion speeds up to 4.9 and 2.2 mm/s, and tether-freeing rates up to 2.9 and 1.8 mm/s, in tabletop conditions and in a colon phantom, respectively.**

***Index Terms*—Mechatronic system, over-the-tube device, pneumatic actuation, robotic endoscopy, soft-tethered colonoscopy.**

I. Introduction

CONVENTIONAL colonoscopy is the golden standard for diagnosis and treatment of colorectal cancer (CRC), namely the development of cancer from colon or rectum, which is the third most diagnosed and second death cause of all types of cancer worldwide. Based on the 2020 statistics reported by the International Agency for Research on Cancer, CRC represents 10% of the 19 million new cancer cases and 9.4% of the 10 million cancer deaths worldwide [1]. Moreover, CRC incidence has been steadily rising, at a global level, over the past years, also because citizens from developing countries nowadays started to adopt a westernized diet and lifestyle [2]. The potential risk factors for CRC growth include obesity, a diet with low intake of fruits and vegetables, less physical exercises, alcohol drinking, and smoking [3]. In order to prevent and reduce the incidence of CRC, besides adopting a healthy lifestyle, regular colonoscopy screening plays a key role in early-stage tumour detection [4]. As a matter of fact, colonoscopy screening and polypectomy reduce the incidence of CRC and mortality [5], and colonoscopy is popularized across the world as one of the most commonly performed and valuable procedures in clinical interventions [6]. However, during conventional colonoscopy, the clinicians introduce the scope through the anus, and excessive pushing/stretching against the colonic wall often causes pain and discomfort [7], which is exacerbated by the well-known looping phenomenon [8].

In order to mitigate the aforementioned issues, researchers are pursuing painless approaches, including robotic colonoscopy systems with multiple functionalities and actuation principles [9], [10], [11]. Amongst them, soft tethers combined with front-wheel navigation, namely tether pulling from tip (i.e., its distal end), represent a promising approach, as demonstrated, e.g., by magnetically driven soft-tethered colonoscopes [12], [13], [14], [15]. Indeed, front-wheel actuation significantly reduces colon stretching and looping, thus fostering high-quality, safe, and painless diagnosis, as well as effective complementary intervention. Yet front-wheel actuation incrementally becomes more challenging as the colonoscope advances, because of the correspondingly increasing contact interactions between tether

Manuscript received 2 February 2023; revised 11 May 2023 and 7 August 2023; accepted 21 September 2023. Recommended by Technical Editor C. Xiong and Senior Editor K. Oldham. This work was supported by the European Commission within the framework of the H2020 European Endoo Project under Grant 688592. *(Yu Huan and Xuyang Ren are co-first authors.) (Edoardo Sinibaldi and Gastone Ciuti share last (senior) authorship.) (Corresponding authors: Xuyang Ren; Gastone Ciuti; Edoardo Sinibaldi.)*

Yu Huan, Xuyang Ren, Andrea Firrincieli, Matteo Cianchetti, and Gastone Ciuti are with the The BioRobotics Institute, Scuola Superiore Sant'Anna, 56127 Pontedera, Italy, and also with the Department of Excellence in Robotics & AI, Scuola Superiore Sant'Anna, 56127 Pontedera, Italy (e-mail: hylsh1314@163.com; xuyang.ren@santannapisa.it; andrea.firrincieli@santannapisa.it; matteo.cianchetti@santannapisa.it; gastone.ciuti@santannapisa.it).

Luigi Manfredi is with the Division of Imaging Science and Technology, School of Medicine, University of Dundee, DD1 4HN Dundee, U.K. (e-mail: l.manfredi@dundee.ac.uk).

Alberto Arezzo is with the Department of Surgical Sciences, University of Torino, 10124 Turin, Italy (e-mail: alberto.arezzo@unito.it).

Edoardo Sinibaldi is with the Istituto Italiano di Tecnologia, 16163 Genoa, Italy (e-mail: edoardo.sinibaldi@iit.it).

This article has supplementary material provided by the authors and color versions of one or more figures available at https://doi.org/10.1109/TMECH.2023.3320429.

Digital Object Identifier 10.1109/TMECH.2023.3320429

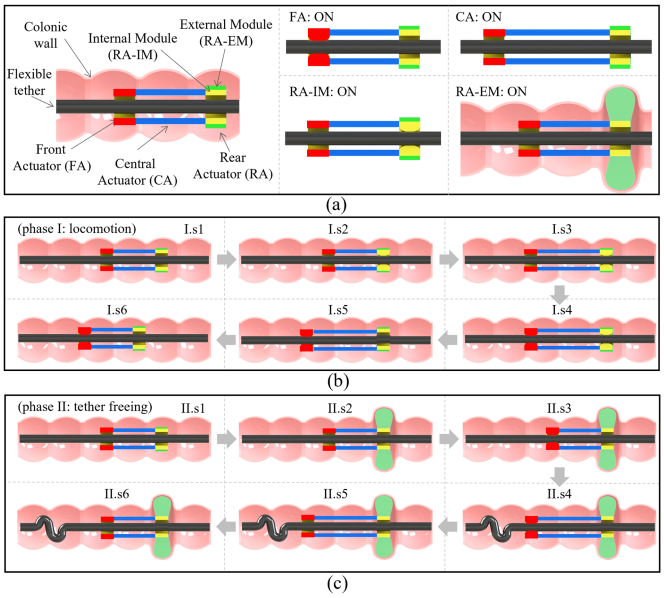

Fig. 1. (a) FOD schematic illustrating its three main functional components: FA (red), CA (blue), and RA (RA-IM yellow, RA-EM green). (b) Operational steps for phase I (locomotion): steps I.s1–I.s6 are cycled in order to make FOD advance along the soft tether (up to a desired working position, in view of the next phase). (c) Operational steps for phase II (tether freeing): after II.s1 and II.s2, steps II.s3–II.s6 are cycled in order to free a sought tether portion.

and the colonic wall, in particular after passing the colonic (splenic and hepatic) flexures. It is worth remarking that such a difficulty hampers front-wheel colonoscopes at large, regardless of the tip-pulling strategy they specifically adopt [16], [17], [18], [19], [20], [21]. Hence, there is a growing quest for strategies and devices aimed at supporting the effective deployment of front-wheel actuated, soft-tethered colonoscopies.

This study tackles the aforementioned challenge by presenting a flexible over-the-tube device (FOD) for tethered colonoscopy. When the pulling force at the endoscope's tip becomes insufficient to overcome the resistance opposing navigation, FOD could be introduced through the anus in order to repeatedly execute a two-phase operation. Specifically, thanks to the selective actuation of four soft pneumatic parts, FOD could first advance along the tether up to a desired working position (phase I: locomotion). Then, upon anchoring to the colonic wall, it could clamp and drag the tether forward (phase II: tether freeing), so as to make available a tether portion ideally subjected to negligible resistive actions, thus restoring the possibility to retake colonoscopy by front-wheel navigation. Focusing on the aforementioned two-phase operation principle, we designed and implemented FOD based on three pneumatic actuators, hereafter labeled as front actuator (FA), central actuator (CA), and rear actuator (RA). Each of them was prototyped and characterized and, upon integration, FOD was successfully validated in tabletop conditions and using an in-vitro colon phantom. Clinical criteria were considered throughout conceptual, design, and testing stages, thanks to close collaboration with experienced clinical specialists also authoring the present study. A related preliminary concept was introduced in the conference article [22], which, however, substantially differs from the present work. Specifically, CA was redesigned by introducing multiple peripheral chambers that do not suffer from inflation instabilities and prevent detrimental contacts between CA and tether/colon. Moreover, in order to reduce the number of engagements with the colonic wall (whence invasiveness) during device locomotion, RA was redesigned by introducing two individually inflatable chambers (with the inner one devised to internally anchor to the tether), thus also preventing hampering effects due to potential backward RA displacements relative to the tether. Furthermore, while the previous conference paper mainly introduced the two-phase working principle, FOD was designed based on specifications that led to a smaller device [in terms of both length and inner/outer diameter (ID/OD)] and tailored operation pressures for FA, CA, and RA (also considering safety limits for interaction with the colonic wall). Finally, for FOD, FA, CA, and RA were quantitatively characterized, and FOD locomotion and tether-freeing performance were quantitatively assessed (also using an advanced colon phantom, whereas a rigid Plexiglas tube was used in the previous article). The present study thus introduces clear conceptual and technical developments compared to [22].

The rest of the article is structured as follows. Section II provides an overview of FOD (including working principle, specifications, and design), while Section III presents system integration. Section IV then reports experimental characterization, whereas Section V presents system validation (for both tabletop and in-vitro tests), prior to discussion, and Section VI provides concluding remarks.

II. System Overview

A. Working Principle: Locomotion and Tether Freeing

From a functional viewpoint, FOD is composed of three pneumatic actuation units, namely FA, CA, and RA. As sketched in Fig. 1(a), when FA is activated, a soft inner membrane is inflated so as to clutch the tether (thus resulting in FA switching from free sliding along the tether to locking on it). When CA is activated, a soft linear actuator is inflated and extended (thus resulting in CA switching from its starting, relatively short length to an extended length). RA features two individually actuated modules: an internal module (RA-IM) and the external module (RA-EM). RA-IM works as FA: upon activation, RA switches from free sliding along the tether to locking on it. Differently, when RA-EM is activated, a soft outer membrane is inflated so as to get in contact with the colonic wall of the local haustra (thus resulting in RA switching from free sliding to anchoring with respect to the colonic wall).

From an operational viewpoint, FOD implements a two-phase procedure. During phase I (locomotion), FOD advances along the tether by a six-step cycle, sketched as I.s1–I.s6 in Fig. 1(b). Specifically, the cycle starts at I.s1, with all three actuators deactivated (and FOD at its initial position along the tether). At I.s2, RA-IM is activated, thus locking on the tether. At I.s3, CA is activated and elongated, thus bringing FA forward along the tether. At I.s4, FA is activated, thus locking on the tether. At I.s5, RA-IM is deactivated, thus unlocking from the tether (whereas

FA still clutches it). At I.s6, CA is deactivated and restores its initial length, thus making FOD advance along the tether. By repeating this six-step cycle, FOD advances up to a desired working position (relatively close to the colonoscope's tip) in view of the next phase. During phase II (tether freeing), FOD takes the six steps sketched as II.s1–II.s6 in Fig. 1(c). Specifically, II.s1 represents the initial status, with all the actuators deactivated. At II.s2, RA-EM is activated, thus anchoring to the colon. At II.s3, FA is activated and locks on the tether. At II.s4, CA is activated and elongates, thus freeing a portion of tether in front of FA. At II.s5, FA is deactivated, thus returning to the condition where it can freely slide along the tether. At II.s6, CA is deactivated, thus returning to its original length. In order to free a sought tether length, steps II.s3–II.s6 are cycled. Finally, after completing the endoscopic procedure, FOD can be either pull out together with the colonoscope or commanded to move back (by reversing its locomotion steps) and exit before pulling out the tether, based on further procedural constraints (including safety and timing).

B. Specifications and Design

Consistent with the current early developmental stage, we addressed a flexible demonstrator with an OD of around 26 mm (representing an average lower anatomical limit [23]) and a length not exceeding 100 mm [24], capable of operating with a soft tether having a diameter up to approximately 10 mm [12]. The targeted size is similar to that of current conventional anoscopes (featuring diameter and length in the range of 15–30 and 65–90 mm, respectively [25], [26], [27]. Moreover, based on previous investigations by the research group [28], we assumed that FOD had to overcome a resistive force $F_r = 2N$. Such a working assumption had to be matched based on the frictional interaction between tether and the colon phantom material considered in the present study. Finally, in view of safety concerns, we assumed the working pressure not to exceed 200 kPa [29], and an upper limit of around 18.5 kPa for the contact pressure with the colonic wall [30], [31], [32].

With reference to the illustration in Fig. 2(a), in order to achieve front-wheel actuation, the pulling force at the colonoscope's tip (F_{tip}) must be able to overcome resistive frictional effects that also increase upon passing the colonic flexures, as described by the following capstan-like model [28]:

$$F_{tip} \geq \left(\left(\Delta F_{S1} e^{\mu\theta_1} + \Delta F_{S2}\right) e^{\mu\theta_2} + \Delta F_{S3}\right) e^{\mu\theta_3} + \Delta F_{S4} \quad (1)$$

where ΔF_{S1}–ΔF_{S4} denote the resistive contributions of segments s_1–s_4, respectively, θ_1–θ_3 represent the angular span of flexures c_1–c_3, respectively, and μ denotes the friction coefficient. Despite the simplifications associated with the underlying model, the expression in (1) highlights how tether deployment is significantly hampered upon incrementally passing the flexures. By assuming quasi-static equilibrium conditions and with reference to the (phase II) free-body diagrams shown in Fig. 2(b), the soft tether is dragged by FA with a force f_{FA} that opposes the resistance F_r: $f_{FA} = F_r$. Moreover, FA is subjected to the reaction force RF_T applied by the tether and to the pushing force F_{CA1} exerted by CA: $F_{CA1} = RF_T$ ($= f_{FA}$). Furthermore, CA is subjected to the reaction force RF_{FA} applied by FA

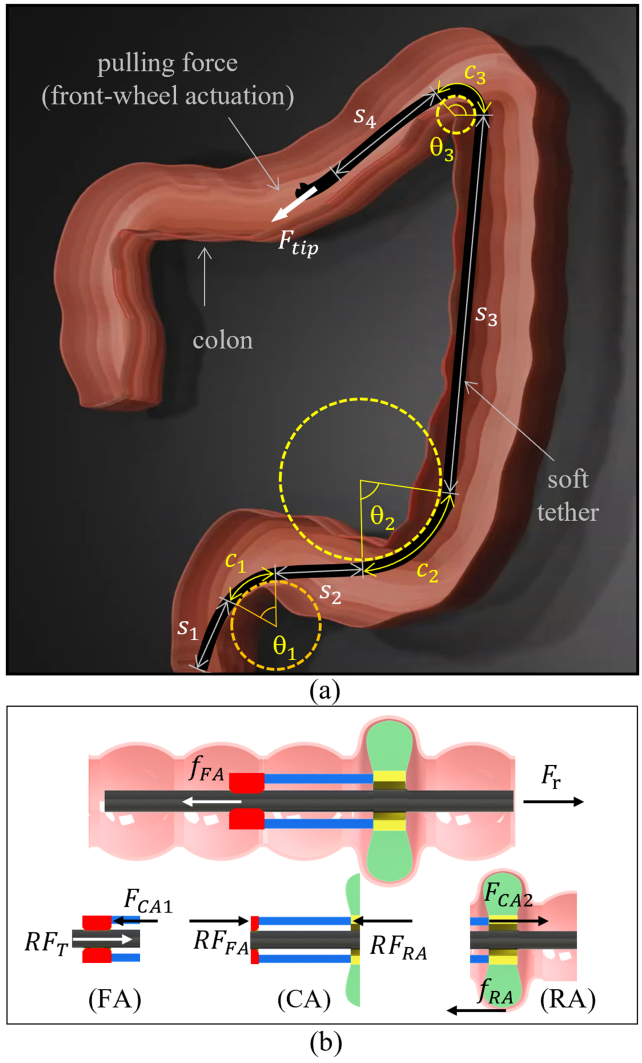

Fig. 2. (a) Schematic of a front-wheel actuated soft-tether colonoscope navigating the colon, with labeling of straight segments s_j and curved segments c_j (flexures). (b) Illustrative phase II free-body diagrams for tether, FA, CA, and RA.

and to the supporting force RF_{RA} exerted by RA: $RF_{RA} = RF_{FA}$ ($= F_{CA1}$). Finally, RA is subjected to the pushing force F_{CA2} applied by CA and to the supporting force f_{RA} exerted by the colon: $f_{RA} = F_{CA2}$ ($= RF_{RA}$).

The conceptual design of the three actuation units FA, CA, and RA (each to be fed by pneumatic lines) is shown in Fig. 3. Specifically, the FA is shown in Fig. 3(a). The exploded view details its components, namely: a sliding ring including three ball bearings and a support frame; a rigid cage; a soft membrane; a rigid cap featuring a passage for the pneumatic feeding line. Moreover, the bottom part of Fig. 3(a) illustrates the related working principle (by means of a cut section): upon pressurization (pressure p in the figure), the soft membrane clutches the tether (through a frictional contact). Finally, in view of the aforementioned dimensional targets, we considered an OD of 26 mm and an ID of 12 mm for FA.

The CA is then shown in Fig. 3(b). The exploded view details its components, namely: a top interface (toward FA); a main body

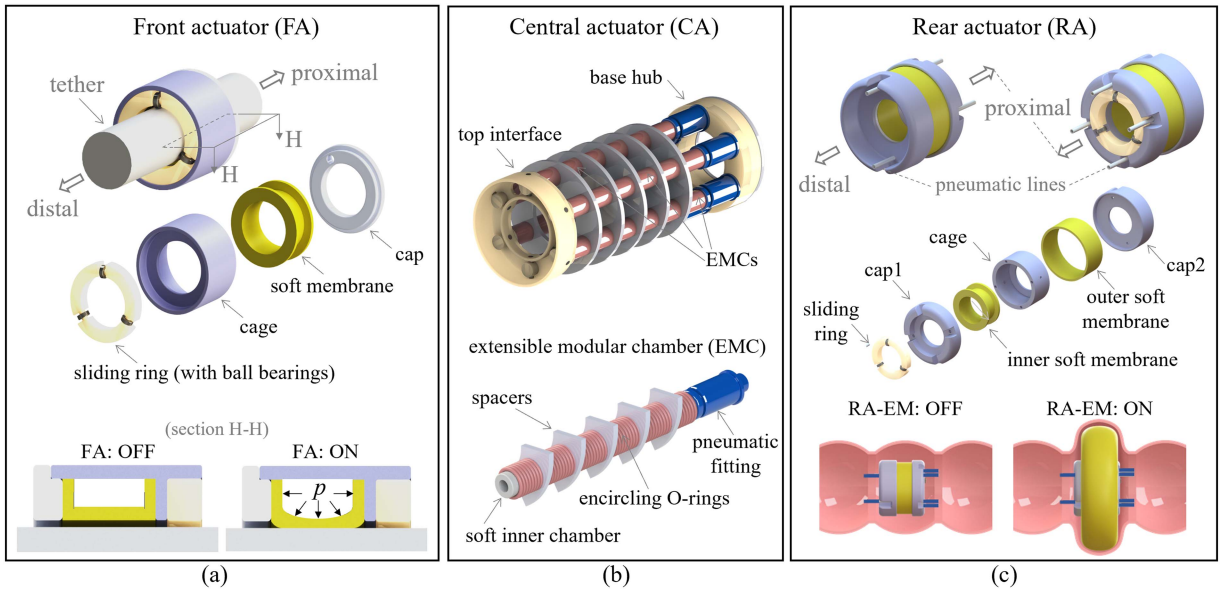

Fig. 3. (a) Design schematic for the FA. Key components are shown through the exploded view; activation by pressurization is sketched through the bottom cut-sectional views. (b) Design schematic for the CA, with a detailed view of the EMC. (c) Design schematic for the RA. Key components are shown through the exploded view; activation by pressurization is sketched, for the external module RA-EM, through the bottom renderings.

composed of a number (n_c) of extensible modular chambers (EMCs); a base hub. As further detailed in the bottom part of Fig. 3(b), each EMC features an inner pneumatic chamber made of soft silicone rubber; encircling O-rings; plastic disk spacers; and a pneumatic fitting functional for assembling. More in detail, the O-rings serve to counteract ballooning potentially occurring due to pressurization, whereas the spacers aim to keep the relative position amongst ECMs and increase structural stability (by increasing the corresponding critical axial load associated with Eulerian instability). Clearly, when the EMCs are pressurized, CA elongates up to a certain extension that depends on the resistive load contextually encountered by FOD.

Considering dimensional constraints in the radial direction and the need to also house O-rings, we considered tentative ID and OD equal to 2 and 4 mm, respectively, for the EMCs. Moreover, by assuming a working pressure in the order of 50 kPa (suitably distant from the aforementioned safety threshold) to act on a disk having a diameter of 3 mm, a pressurization force on the order of 0.35 N is obtained, thus leading to choose $n_c = 6$ EMCs to overcome the target resistive force F_r. Moreover, considering a tentative EMC initial length of around 40 mm, and by assuming a load-free elongation on the order of 10 mm (i.e., order of 10% of the body length) upon 50 kPa pressurization, a Young modulus around 1.8×10^5 Pa is needed for the soft pneumatic chamber inside the EMC. Therefore, we consistently choose to fabricate the EMC chamber with a Dragon Skin 10 NV (Smooth-On, Inc., U.S.A.) silicone [33], [34].

The RA is finally shown in Fig. 3(c). The exploded view details its components, namely: a sliding ring including three ball bearings and a support frame; a rigid cap at the distal end (cap1); an inner soft membrane; a rigid cage; an outer soft membrane; a rigid cap at the proximal end (cap2). Pneumatic lines are also hinted (four input lines at the proximal section; two output lines at the distal section, for transmission to CA and FA). Moreover, the bottom part of Fig. 3(c) illustrates the working principle for module RA-EM (RA-IM being identical to FA, as anticipated): upon pressurization, the outer soft membrane engages with the local colonic haustra. Specifically, in order not to exceed the aforementioned safety threshold (of around 18.5 kPa for contact with the colonic wall), we devised to operate RA-EM with 15 kPa pressure.

III. System Integration

A. System Prototyping

The assembled FOD system is shown in Fig. 4(a). Let us preliminarily observe that, for ease of prototyping, the pneumatic lines were implemented through polyvinyl chloride (PVC) tubes (ID: 1.6 mm, OD: 2 mm) with the only exception of that one for FA, which was implemented by wrapping a silicone tube extension around CA (considering extra length to allow for elongation).

The FA and RA soft membranes, as well as the inner chambers of the EMCs in CA, were molded with silicone rubber materials: Dragon Skin 20 for FA and RA-IM, Ecoflex 00-30 for RA-EM, and Dragon Skin 10 NV for the EMCs. In particular, for RA-EM we chose a relatively more compliant material such as Ecoflex 00-30 in order to enhance extended deformation, as required to conform to the haustra geometry. Moreover, for the membranes devised to clamp the tether we chose Dragon Skin 20, rather than Dragon Skin 10 NV, because of its higher frictional coefficient (as resulting from characterization tests similar to those performed for the FA clamping force, see Section IV). Degassing of the silicone was performed by using a VTR5022 vacuum machine (Heraeus, Germany), after that curing was performed at room temperature. Furthermore, all the involved molds (for FA, CA, and RA) were 3D printed with VisiJet M3 Crystal (ProJet MJP 3600, 3D systems, Inc., USA).

As concerns FA, the sliding ring frame, the cage, and the cap were 3D-printed. Three ball bearings (ID: 1 mm, OD: 3 mm;

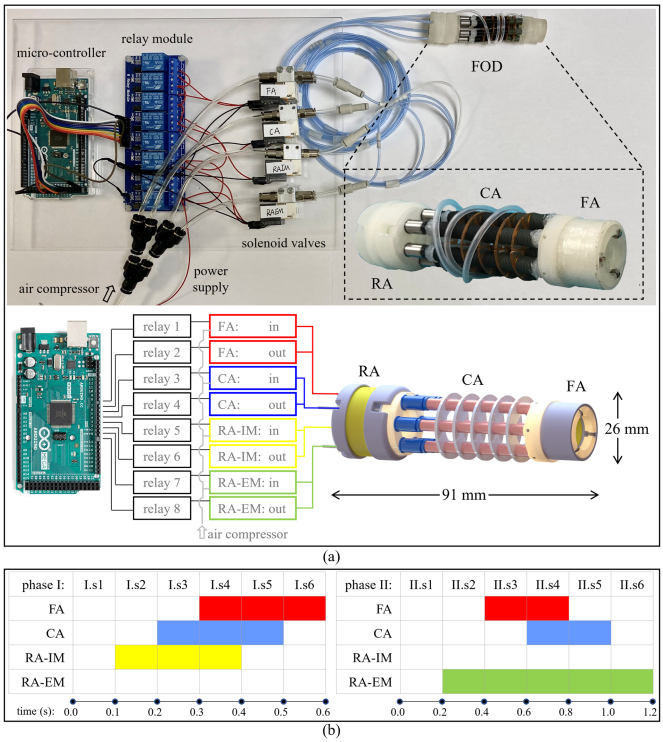

Fig. 4. (a) Integrated FOD system, including the electro-pneumatic control unit. Top: physical implementation; bottom: corresponding electrical scheme. (b) Time-activation sequence for FA, CA, RA-IM, and RA-EM (colored/empty cells stand for activated/idle states), for both phase I and phase II (steps labeled as in Fig. 1).

MISUMI, Inc., Japan) were fixed on the frame by means of 1 mm diameter metal pins. The 1 mm-thick soft membrane was sealed to cage and cap via Loctite 4011 glue (Henkel Corp., USA); the pressure line was similarly sealed to the cap. Upon assembly, FA resulted in a diameter of 20 mm and a length of 15 mm.

Furthermore, as regards CA, top interface and base hub were 3D-printed, and each EMC was molded (ID: 2 mm, OD: 4 mm, length: 40 mm) and encircled with O-rings (ID: 4 mm, OD: 5 mm). Moreover, five PVC disks were evenly interleaved with O-rings in order to increase structure stability, as discussed above. The disks were obtained from a 1 mm thick plate by means of a VLS3.50 laser cutter (Universal Laser Systems, Inc., USA). Furthermore, each EMC was glued to the FA, whereas a pneumatic fitting (diameter: 5 mm, length: 10 mm; MISUMI, Inc., Japan) was introduced to connect the EMC to the CA. More in detail, an auxiliary PTFE tube chunk (ID: 0.8 mm, OD: 1.2 mm) was glued to the EMC and inserted into the fitting. Upon assembly, CA resulted in a diameter of 23 mm and a length of 56 mm.

Finally, as concerns RA, the sliding ring frame, the cage, and the caps were 3D-printed, and three ball bearings were fixed on the sliding ring frame as for FA. Moreover, the inner and outer soft membranes were glued and sealed to cage and caps. In addition, four PTFE tube chunks were inserted and glued in cap2 (upon which the input pressure lines were press-fit), and two chunks were inserted and glued into cap1 (devised to transmit pressure to the CA base hub and the silicone tube extension reaching FA). Upon assembly, RA resulted in a diameter of 26 mm and a length of 20 mm.

After all three actuators had been properly assembled, air tightness was checked in order to proceed with subsequent characterization.

B. Electro-Pneumatic Control Unit

The electro-pneumatic control unit shown in Fig. 4(a) was developed for operating FOD. Specifically, the considered unit consists of a microcontroller (Arduino Mega 2560), an eight-channel relay module, eight two-way (normally closed) solenoid valves (N3-HIGHEND, Hangzhou, China) operated at 12 Vdc, a mini air pump (KMDP-U3, KAIMENG, Shenzhen, China) operated at 12 Vdc, besides pneumatic connectors and tubes. Each of the four pneumatic actuators (namely FA, CA, RA-IM, and RA-EM) was pneumatically connected to two solenoid valves. For ease of development, open-loop pressure control was implemented, based on valve activation timing. When 12 Vdc is individually supplied, one solenoid valve drains air from the mini pump and serves as air inlet, while the other valve serves as air outlet. When the voltage is removed, both solenoid valves are closed, and the corresponding chamber pressure is maintained. Furthermore, a 0.6 s period and a 0.8 s period were coded for the cyclic steps foreseen for phase I (locomotion) and phase II (tether freeing), respectively, according to the time sequences sketched in Fig. 4(b), where colored/empty cells denote activated/idle states for each actuator.

IV. Experimental Characterization

Each actuator (namely FA, CA, and RA) was individually characterized; hereafter, methods and results are jointly reported, for ease of presentation. As regards RA, only the RA-EM module was considered (being RA-IM identical to FA).

As regards FA, we characterized the tether clamping force by using a commercial tensile tester Instron 5965 (Instron, USA). We used a soft polyurethane tether (OD: 8 mm), filled with five tubes (SMC Corporation, Japan) to mimic the geometry and structural stiffness of a conventional colonoscope while considering the basic functionalities (namely operative channel, electrical wires, insufflation, irrigation, and flushing), as done in [12]. As shown in Fig. 5(a), FA was initially caged and clamped through the lower tester grip, while the upper grip, connected to the tester moving stage and equipped with a load cell (Instron 4464, Norwood, USA), was used to clamp the free end of the tether. FA was then pressurized at 50, 100, and 150 kPa, and for each pressure value, the moving stage was raised for 10 mm at 0.5 mm/s. Each test was performed thrice. The obtained readout force is shown in Fig. 5(b): the maximum tether-clutching forces (namely those before slippage occurred) corresponding to the aforementioned pressure values were 0.6, 1.9, and 3.7 N. In view of the obtained results and considering the target resistive force ($F_r = 2N$), we selected a pressure value of 150 kPa to operate FA (as well as RA-IM), thus also keeping a safety margin with respect to 200 kPa potentially harmful for operation [21].

As for CA, we characterized both the pushing force and the load-free elongation associated with pressurization. Specifically, a horizonal load cell (HP 30, Yueqing Handpi Instruments Co., Ltd., Zhejiang, China) was used for measuring the pushing force, once clamped the CA base through a fastening interface as in

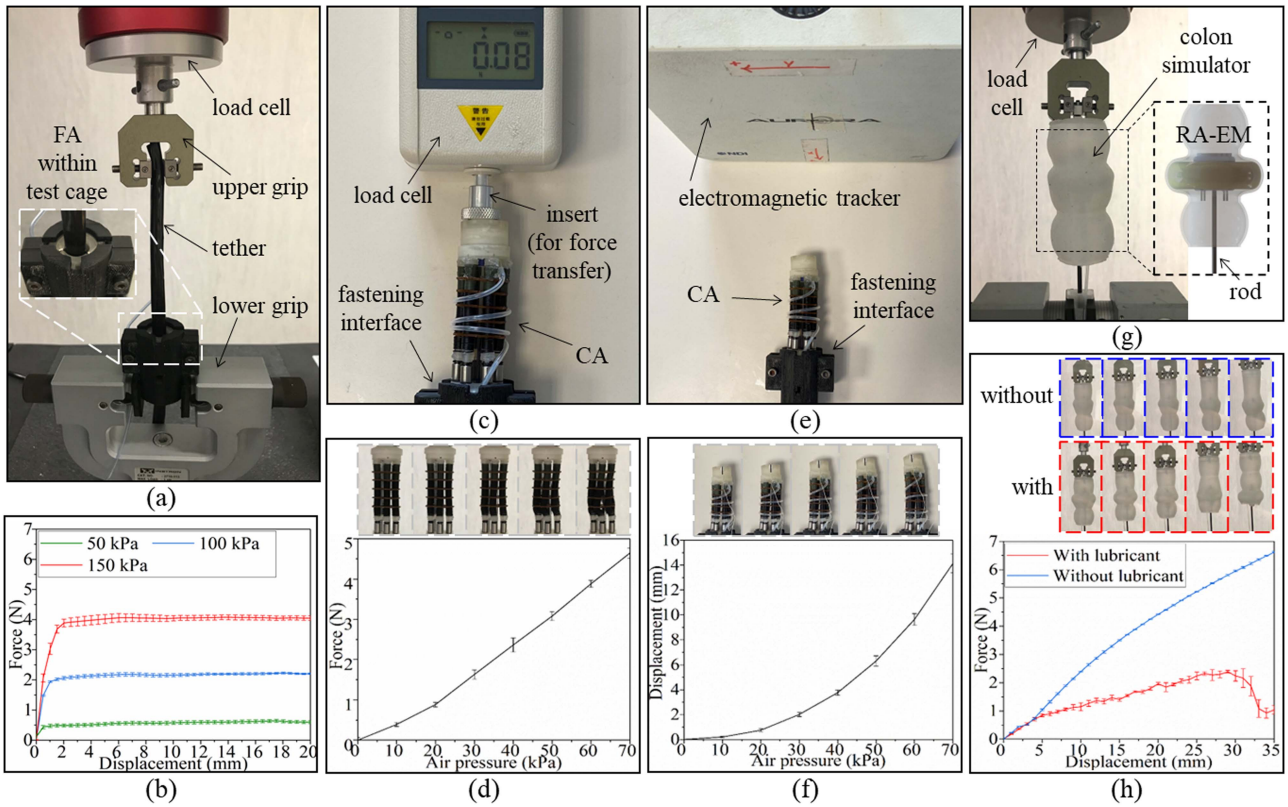

Fig. 5. Experimental characterization: setups and related results. (a) Test setup for the tether-clutching force exerted by FA (as well as RA-IM). (b) Corresponding results for selected pressurization values. (c) Test setup for the pushing force exerted by CA. (d) Corresponding results. (e) Test setup for the load-free CA elongation. (f) Corresponding results. (g) Test setup for the anchoring force exerted at 15 kPa inflation pressure by RA-EM. (h) Corresponding results with and without colon lubrication. For all the experiments, error bars represent one standard deviation over three replicates.

Fig 5(c), whereas an electromagnetic tracker (Northern Digital Inc., Aurora, Canada) was used to record the tip elongation as shown in Fig 5(e). The input pressure was varied from 0 to 70 kPa (to investigate an extended pressure range compared to the working value assumed during the conceptual design phase) with steps of 10 kPa, and each test was repeated thrice. The force results, reported in Fig. 5(d), confirmed that a working pressure of 50 kPa was sufficient to counteract the target resistive force F_r. Furthermore, as shown in Fig 5(f), the load-free elongation at 50 kPa was nearly 6 mm, which is compatible with the underlying design assumptions in view of actual material properties and nonideal operation conditions (for which, e.g., some fraction of the pressurizing work is not perfectly transduced into one-dimensional EMC extension).

Finally, as concerns RA, we assessed the anchoring performance of RA-EM by using the aforementioned tester machine. To this purpose, we also fabricated (by molding) a simulator of a straight colon segment (length: 90 mm, diameter; 30/40 mm with/without haustra) using Ecoflex 00-30 as in [35]. The friction coefficient between polyurethane tether and Ecoflex 00-30, namely 0.126 ± 0.016, was very close to that reported in [28], thus corroborating the resistive force adopted to ice-break design. More in detail, the RA was firmly connected to the tester base through a rigid rod, as shown in Fig 5(g), whereas the moving stage was connected to the colon simulator. After pressurizing the involved soft membrane at 15 kPa, we commanded the sensorized stage to raise for 35 mm at 0.5 mm/s. To characterize the system closer to realistic working conditions, we performed the experiments by also lubricating the colon with Vaseline oil (Alvita, Italy), thus also considering less conservative working conditions. Each test was performed thrice. As shown in Fig. 5(h), although lubrication introduced a dramatic effect on the anchoring performance, RA managed to effectively anchor to the colon, being able to sustain a traction force around 2.4 N, thus above the target resistive force F_r.

V. System Validation

FOD was validated in terms of both locomotion and tether-freeing capabilities; hereafter, methods and results are jointly reported, for ease of presentation. More in detail, a preliminary performance assessment was carried out considering simplified tabletop conditions. Then, FOD operation was validated in an in-vitro colon phantom, thus considering working conditions closer to the perspective medical scenario. For all the carried-out tests, and based on previous characterization, we operated FA (as well as RA-IM), CA, and RA-EM at pressures equal to 150, 50, and 15 kPa, respectively. To this purpose, using a common inlet pressure of 282 kPa, the valve activation times were set to 0.018, 0.059, and 0.140 s, for CA, FA (as well as RA-IM), and RA-EM, respectively.

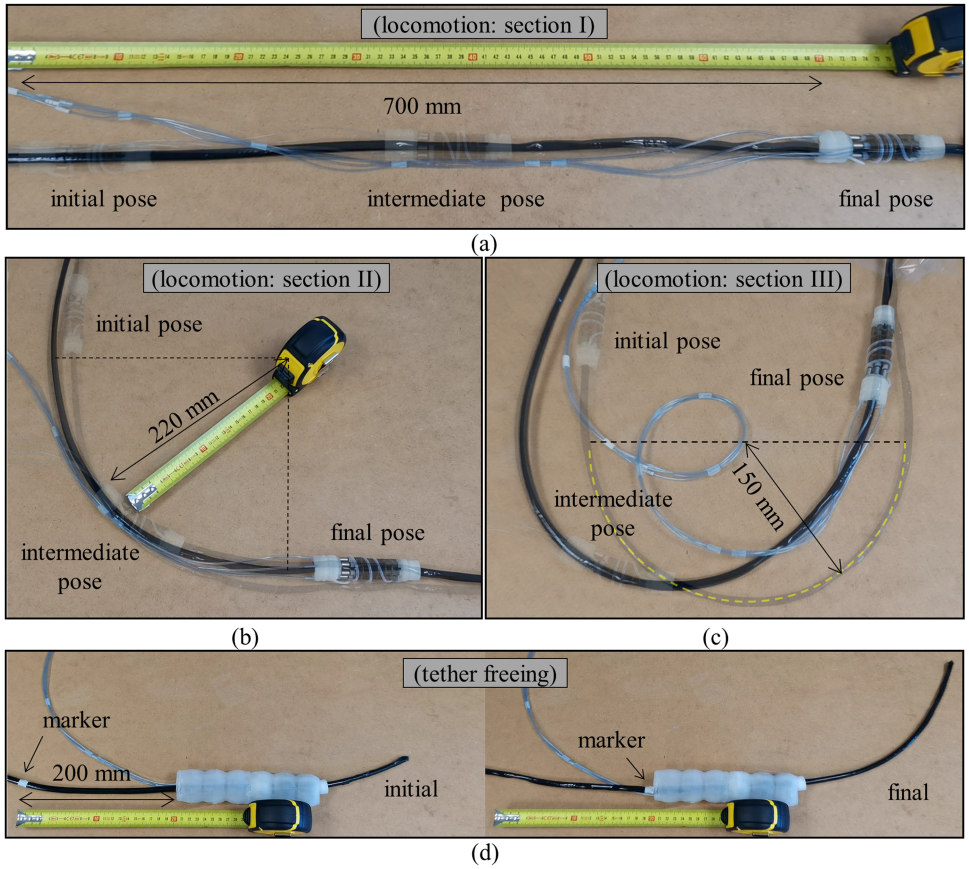

Fig. 6. Experimental validation in tabletop conditions. (a) Locomotion test along a straight tether section. (b) Locomotion test along a curved (90 deg turning) tether section. (c) Locomotion test along a curved (180 deg turning) tether section. (d) Tether freeing test. Image overlays are used to show FOD initial, intermediate, and final poses in the locomotion tests, which were accomplished with average speeds of 4.9 (Section I), 3.1 (Section II), and 2.9 mm/s (Section III). Tether freeing was accomplished at an average rate of 2.9 mm/s.

A. Validation in Tabletop Conditions

As regards locomotion, FOD was commanded to advance along three tether sections representative of different colonic tracts. In particular, we considered: a straight tether section (Section I; length: 700 mm); a 90 deg turning section (Section II; length: 400 mm, radius of curvature: 220 mm); a 180 deg turning section (Section III; length: 500 mm, radius of curvature: 150 mm). For each test case, we measured the average locomotion speed.

The initial and final FOD poses, together with an intermediate one, are shown (also using overlays) in Fig. 6(a), (b), and (c) for Sections I, II, and III, respectively. In Sections I, II, and III, FOD advanced over the corresponding length in 143, 128, and 172 s, respectively, thus resulting in corresponding average locomotion speeds of 4.9, 3.1, and 2.9 mm/s. We observe that some tether displacements were caused by FOD advancement in Section III because of the relatively sharp turning over the unconstrained tether; however, the relative speed with which FOD advanced along the tether was substantially unaltered by tether displacement, thus supporting the carried-out experimental measurements.

As regards tether freeing, FOD was placed inside a 180 mm-long straight colon simulator segment (similar to the one introduced in Section IV), and RA-EM was activated so as to anchor to the colonic wall. Once inserted the tether, FOD was commanded to free a 200 mm-long tether portion, as identified by a marker on the tether itself, and we finally measured the average rate at which the tether was freed.

The initial and final tether positions are shown in Fig. 6(d), where the marker is also visible. FOD completed the task in 68 s, resulting in an average tether-freeing rate of 2.9 mm/s.

FOD performance in tabletop conditions is further illustrated through Supplementary Video S1.

B. Validation in In-Vitro Colon Phantom

Both locomotion and tether-freeing FOD capabilities were further assessed by means of a complete in-vitro colon phantom, which was fabricated similarly to the colon segment introduced in section IV. More in detail, in order to demonstrate FOD capabilities in an integrated way, we considered the clinically representative challenge of overcoming the splenic and the hepatic flexures with a front-wheel actuated colonoscope.

Consistently, and with reference to Fig. 7(a), we, thus, first considered a first scenario (scenario I) where the tip of a front-wheel colonoscope is stuck in proximity of the splenic flexure (as hinted through the dashed tip overlay in the figure). In such a circumstance, FOD effectively advanced over the tether toward the colonoscope's tip, up to a working position closer to the tip

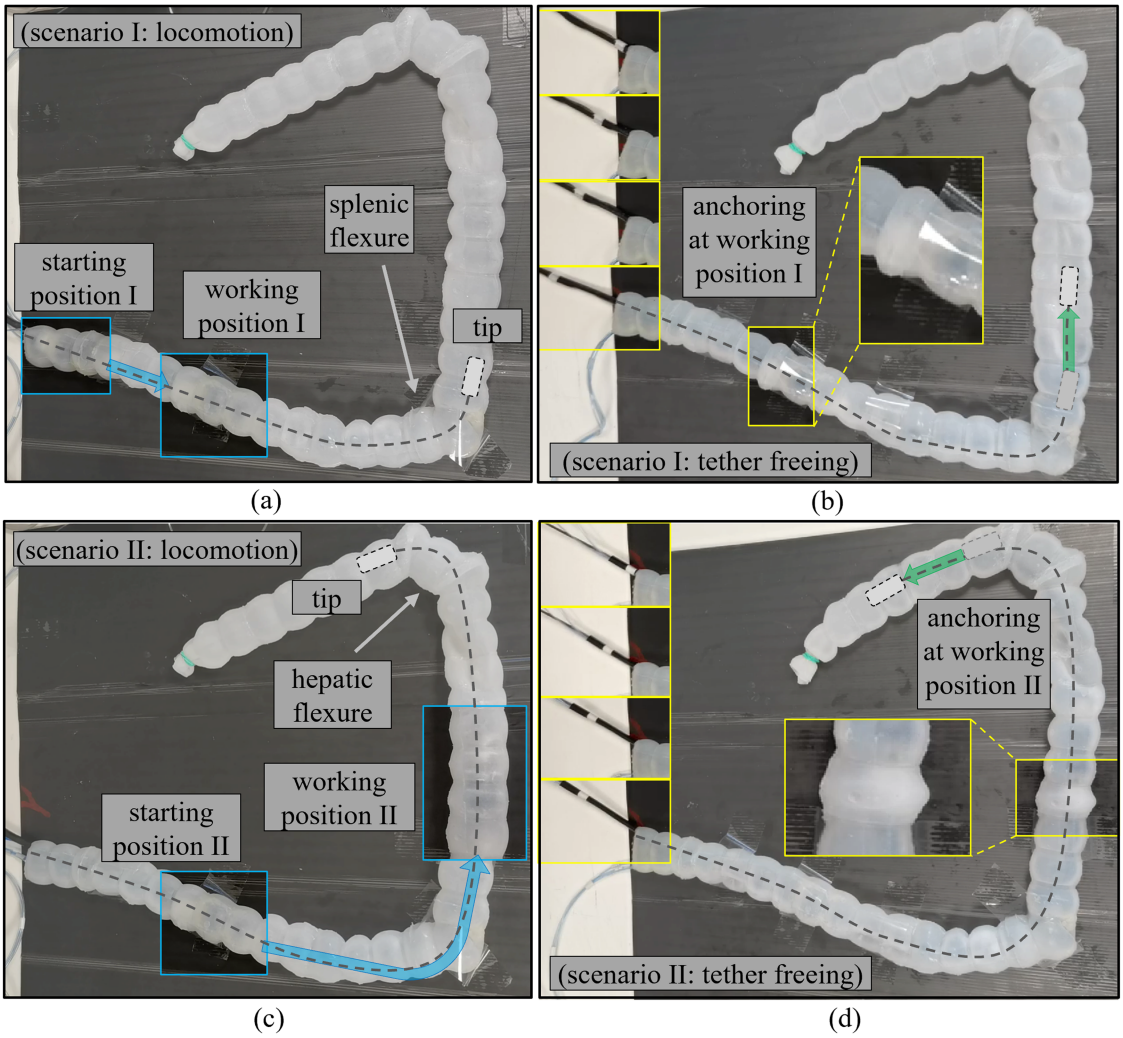

Fig. 7. Experimental validation in an in vitro colon simulator. Scenario I (colonoscope's tip stuck close to the splenic flexure): (a) locomotion up to a working position, from where (b) tether freeing is performed. Scenario II (tip stuck close to the hepatic flexure): (c) locomotion up to a working position, from where (d) tether freeing is performed. Tether freeing is detailed in (b) and (d) through incremental marker displacements in the insets.

(namely in the descending colon segment in the figure at hand). Once anchored to the local haustra, FOD was able to effectively free the tether as shown through the insets in Fig. 7(b), thus allowing the colonoscope to further advance along the transverse colon segment (as hinted in the figure).

Moreover, with reference to Fig. 7(c), we then considered a second scenario (scenario II) where the colonoscope's tip is stuck in proximity of the hepatic flexure. In such a circumstance, FOD reached a working position in the transverse colon segment and, once anchored therein, it successfully freed the tether as shown through the inserts in Fig. 7(d), thus enabling further navigation toward the caecum (as hinted in the figure).

For both scenarios I and II, FOD successfully accomplished the locomotion and tether-freeing tasks, while also demonstrating a flawless operation when advancing over the splenic flexure. More in detail, FOD advanced with an average locomotion speed of 2.2 mm/s (scenario I) and 1.9 mm/s (scenario II), and its tether freeing rate was equal to 1.8 mm/s (scenario I) and 1.1 mm/s (scenario II). FOD performance in the in-vitro colon phantom is further illustrated through Supplementary Video S2. For the sake of clarity, let us remark that, in order to enable colonoscope tip advancement in a chosen colonic tract, it is not required that FOD reach that tract. It is sufficient that FOD anchors at a previous tract and frees tether therein, so that the as-freed tether enables subsequent front-wheel pulling in the chosen tract. With the reference to Supplementary Video S2, for instance, in order to enable front-wheel colonoscope actuation in the caecum, FOD is called to reach the transverse colonic tract, and free tether therein (i.e., FOD is not asked to reach the caecum). In order to further illustrate this point and augment FOD validation, we considered a magnetically driven soft-tethered colonoscope, obtained by integrating a magnetic endoscopic capsule at tether's tip, to be pulled by means of an external permanent magnet (supported by a common Martin's arm, for simplicity). We then used FOD, in particular, to free the tether (upon anchoring to the transverse colon) as needed for the magnetic capsule to overcome the hepatic flexure and approach the caecum along the ascending colon. Such a complementary illustration is included in Supplementary Video S2 (as "bonus material," given the study focus on FOD rather than magnetically driven colonoscopy). Moreover, in order to further emphasize FOD capabilities, the final section of Supplementary Video S2 shows that even FOD

itself is able to overcome the hepatic flexure and move in the ascending tract. As remarked above, however, FOD is not devised to perform such an extra-procedural task, which is shown for the sake of extended illustration. Finally, endoscopic sequences are shown at the beginning of Supplementary Video S2, aimed at providing the reader with complementary internal views of FOD locomotion and tether freeing.

VI. Discussion and Concluding Remarks

A flexible mechatronic device for front-wheel soft-tethered colonoscopy was conceived, prototyped, characterized, and preliminary validated up to in-vitro colon phantom tests.

The proposed device, concisely labeled as FOD in the present manuscript, supports soft-tethered colonoscopy by means of a two-phase operation: locomotion over the tether (phase I) and subsequent tether freeing (phase II). FOD features a diameter of 26 mm and a length of 91 mm, and it is operated by using pressure of 150, 50, and 15 kPa for the FA (which is the same as the internal module of the RA, i.e., RA-IM), the CA, and the external module of the RA (RA-EM), respectively.

Thanks to the use of compliant materials (namely, rubber elastomers, also complemented with elastic and metallic elements), FOD is able to conform to the colon anatomy while advancing and to respectfully engage with the colonic wall upon anchoring. Moreover, the chosen pressures permit to overcome the targeted resistive force (2N) while also remaining below the 200 kPa threshold for safe operation within the colon [29], and the 18.5 kPa threshold for safe contact with its wall [30]. Furthermore, FOD was successfully tested both in tabletop conditions and in an in-vitro realistic colon phantom. Specifically, the assistive device was able to advance over the tether, even along curved tracts (including 180 deg turnings), and to successfully overcome anatomical challenges such as the splenic flexure in the colon phantom, by featuring speeds between 2.9 and 4.9 mm/s for tabletop tests and between 1.9 and 2.2 mm/s for colon phantom tests. In addition, FOD was capable to effectively free the tether with rates of 2.9 mm/s for tabletop tests, and between 1.1 and 1.8 mm/s for colon phantom tests. FOD operation was further illustrated by assisting a magnetically driven soft-tethered colonoscope in approaching the phantom's caecum. In this regard, it is worth remarking that the proposed in-vitro simulator, recently published by the authors, together with extended contributions, in a specifically focused paper [36], provides an unprecedented setting to test endoscopic robots. Indeed: it reproduces human anatomical conditions reconstructed from CT colonography images and literature data; it represents haustra and muscular tones (missing in human cadavers), thus enabling conformational contact; it simulates realistic frictional contact (as demonstrated since [28]). Moreover, while preserving the aforementioned desired characteristics, it is advisable to develop simulators with enhanced optical transparency, for ease of experimental characterization.

Considering the starting functional specifications, we thus successfully developed the sought device, in particular through an embodiment that is compatible, in terms of size and operational pressure, with clinical applications. Collaboration with clinical specialists, in particular, was key for targeting a prototype with a size similar to that of current conventional anoscopes, thus paving the way for potential translation. Moreover, in view of the reported speeds, FOD would be able to travel along, e.g., a 140 cm long colon tract, in around 12 min, thus compatibly with procedural times.

FOD is substantially different from prior over-the-tube assistive devices, such as Endo-Ease Discovery [37] and Pathfinder [38]. FOD is a relatively short compliant device that is conceived to move along soft tethers, whereas previous devices (having a characteristic length around 100 cm) are steadily mounted at the distal section (close to tip) of conventional (less flexible) colonoscope shafts. This reflects the intrinsically different underlying assistive concept: while Endo-Ease Discovery and Pathfinder were devised to support the deployment of a conventional colonoscope from its base, through manual corkscrew insertion (to leverage frictional effects on colonic wall) and stiffening (to mitigate looping), respectively, FOD was conceived to move along and free soft tethers used in front-wheel colonoscopy. Consistently with above, FOD is expected to be more compliant than prior-art devices, yet any related differences, particularly in interaction force with colon, could be quantitatively assessed at a later developmental stage, and based on specific sensorization even for prior-art devices.

However, the current FOD prototype still requires improvements. In particular, further miniaturization has to be accomplished in order to foster clinical translation. In this regard, it is worth observing that based on discussions with clinical partners, FOD could be inserted into and retrieved from the rectal sphincter by the physician, thanks to its compliant structure; based on further miniaturization, it could be retrieved by locomotion (using a time-reversed control law) or as clamped to the tether (by possibly pulling the pneumatic lines as well). However, stronger claims must be backed by subsequent focused experiments, possibly involving advanced phantoms including a physically/clinically representative sphincter tract. Nonetheless, the tether will support both FOD insertion and retrieval by providing a physical track (thus avoiding, e.g., uncontrolled bending and kinking), and FOD and tether miniaturization may go hand in hand toward increasingly painless front-wheel colonoscopy. Moreover, system sealing should be implemented through a compliant skin, while also using fully biocompatible materials. In this regard, the implementation of the pneumatic system should be refined (yet the fact that most of the electro-pneumatic components are devised to be external to the body supports effective development closer to pre-clinical test conditions). Closed-loop pressure control should be implemented, by negotiating system complexity with pressure sensing capabilities and by possibly including sensors/methods for estimating contact pressure between RA-EM and colonic wall, so as to enforce effective-and-safe anchoring. Moreover, anchoring should be further assessed by using physical simulators with spatially varied diameters, although patient-specific variability could be alternatively faced by introducing a family of FOD devices, e.g., differing from one another for their diameter, so as to tailor a specific FOD to a certain patient based on preoperative imaging. In addition, system modeling should be consistently refined by negotiating accuracy and complexity, based on model objectives and calibration data. Furthermore, whether to further develop

the system to be reusable (upon sterilization) or disposable, should be carefully analyzed based on further evaluations and considering cost-effectiveness. Finally, it is worth underlining that FOD has potential for clinical translation, since it could effectively enact painless front-wheel colonoscopy. However, more accurate and stronger claims should be based on extensive tests, also in ex-vivo and in-vivo conditions. In this regard, human tests could be reached in 5–10 years, as needed to increase the device technology readiness level, also depending on possible liaison with clinical institutions and investments.

Nonetheless, it is worth remarking that the developed device could be used with (and further customized for) a variety of soft-tethered colonoscopes, thus amplifying its potential impact in the search for effective minimally invasive interventional strategies against CRC.

Acknowledgment

The authors would like to thank Nicodemo Funaro for 3D printing of relevant prototype components

References

[1] H. Sung et al., "Global cancer statistics 2020: GLOBOCAN estimates of incidence and mortality worldwide for 36 cancers in 185 countries," *CA, A Cancer J. Clinicians*, vol. 71, pp. 209–249, Feb. 2021, doi: 10.3322/caac.21660.

[2] P. Rawla, T. Sunkara, and A. Barsouk, "Epidemiology of colorectal cancer: Incidence, mortality, survival, and risk factors," *Przeglad Gastroenterologiczny*, vol. 14, no. 2, pp. 89–103, 2019, doi: 10.5114/pg.2018.81072.

[3] N. N. Keum and E. Giovannucci, "Global burden of colorectal cancer: Emerging trends, risk factors and prevention strategies," *Nature Rev. Gastroenterol. Hepatol.*, vol. 16, no. 12, pp. 713–732, Dec. 2019, doi: 10.1038/s41575-019-0189-8.

[4] M. Song and A. T. Chan, "Environmental factors, gut microbiota, and colorectal cancer prevention," *Clin. Gastroenterol. Hepatol.*, vol. 17, no. 2, pp. 275–289, Jan. 2019, doi: 10.1016/J.CGH.2018.07.012.

[5] M. F. Kaminski, D. J. Robertson, C. Senore, and D. K. Rex, "Optimizing the quality of colorectal cancer screening worldwide," *Gastroenterology*, vol. 158, no. 2, pp. 404–417, Jan. 2020, doi: 10.1053/j.gastro.2019.11.026.

[6] E. Dekker and D. K. Rex, "Advances in CRC prevention: Screening and surveillance," *Gastroenterology*, vol. 154, no. 7, pp. 1970–1984, May 2018, doi: 10.1053/j.gastro.2018.01.069.

[7] S. Singla et al., "Splenic injury during colonoscopy-a complication that warrants urgent attention," *J. Gastrointestinal Surg.*, vol. 16, no. 6, pp. 1225–1234, Jun. 2012, doi: 10.1007/S11605-012-1871-0/TABLES/4.

[8] A. Loeve, P. Breedveld, and J. Dankelman, "Scopes too flexible and too stiff," *IEEE Pulse*, vol. 1, no. 3, pp. 26–41, Nov./Dec. 2010, doi: 10.1109/MPUL.2010.939176.

[9] L. Manfredi, *Endorobotics: Design, R&D and Future Trends*. Cambridge, MA, USA: Academic 2022.

[10] G. Ciuti et al., "Frontiers of robotic colonoscopy: A comprehensive review of robotic colonoscopes and technologies," *J. Clin. Med.*, vol. 9, no. 6, 2020, Art. no. 1648, doi: 10.3390/jcm9061648.

[11] W. Marlicz et al., "Frontiers of robotic gastroscopy: A comprehensive review of robotic gastroscopes and technologies," *Cancers (Basel)*, vol. 12, no. 10, 2020, Art. no. 2775, doi: 10.3390/cancers12102775.

[12] M. Verra et al., "Robotic-assisted colonoscopy platform with a magnetically-actuated soft-tethered capsule," *Cancers (Basel)*, vol. 12, no. 9, 2020, Art. no. 2485, doi: 10.3390/cancers12092485.

[13] J. W. Martin et al., "Enabling the future of colonoscopy with intelligent and autonomous magnetic manipulation," *Nature Mach. Intell.*, vol. 2, no. 10, pp. 595–606, Oct. 2020, doi: 10.1038/s42256-020-00231-9.

[14] Y. Li et al., "Design and preliminary evaluation of an electromagnetically actuated soft-tethered colonoscope," *IEEE Trans Med Robot Bionics*, vol. 3, no. 2, pp. 402–413, May 2021, doi: 10.1109/TMRB.2021.3063844.

[15] J. C. Norton et al., "Intelligent magnetic manipulation for gastrointestinal ultrasound," *Sci. Robot.*, vol. 4, no. 31, Jun. 2019, Art. no. eaav7725, doi: 10.1126/SCIROBOTICS.AAV7725/SUPPL_FILE/AAV7725_SM.PDF.

[16] L. Manfredi, E. Capoccia, G. Ciuti, and A. Cuschieri, "A soft pneumatic inchworm double balloon (SPID) for colonoscopy," *Sci. Rep.*, vol. 9, no. 1, 2019, Art. no. 11109, doi: 10.1038/s41598-019-47320-3.

[17] M. Quirini, R. J. Webster, A. Menciassi, and P. Dario, "Design of a pill-sized 12-legged endoscopic capsule robot," in *Proc. IEEE Int. Conf. Robot. Automat.*, 2007, pp. 1856–1862. doi: 10.1109/ROBOT.2007.363592.

[18] J. E. Bernth, A. Arezzo, and H. Liu, "A novel robotic meshworm with segment-bending anchoring for colonoscopy," *IEEE Robot. Automat. Lett.*, vol. 2, no. 3, pp. 1718–1724, Jul. 2017, doi: 10.1109/LRA.2017.2678540.

[19] Q. Zhang, J. M. Prendergast, G. A. Formosa, M. J. Fulton, and M. E. Rentschler, "Enabling autonomous colonoscopy intervention using a robotic endoscope platform," *IEEE Trans. Biomed. Eng.*, vol. 68, no. 6, pp. 1957–1968, Jun. 2021, doi: 10.1109/TBME.2020.3043388.

[20] J. Chen et al., "A novel inchworm-inspired soft robotic colonoscope based on a rubber bellows," *Micromachines*, vol. 13, no. 4, Apr. 2022, Art. no. 635, doi: 10.3390/MI13040635.

[21] E. Tumino et al., "Use of robotic colonoscopy in patients with previous incomplete colonoscopy," *Eur. Rev. Med. Pharmacological Sci.*, vol. 21, no. 4, pp. 819–826, Feb. 2017. Accessed: Jan. 19, 2023. [Online]. Available: https://europepmc.org/article/med/28272700

[22] N. Gabrieli, J. O. Alcaide, M. Cianchetti, A. Menciassi, and G. Ciuti, "A novel soft device for assisting magnetically-driven soft-tethered capsule navigation," in *Proc. IEEE Int. Conf. Cyborg Bionic Syst.*, 2019, pp. 261–265. doi: 10.1109/CBS.2018.8612284.

[23] A. Alazmani, A. Hood, D. Jayne, A. Neville, and P. Culmer, "Quantitative assessment of colorectal morphology: Implications for robotic colonoscopy," *Med. Eng. Phys.*, vol. 38, no. 2, pp. 148–154, Feb. 2016, doi: 10.1016/j.medengphy.2015.11.018.

[24] F. Cosentino, E. Tumino, G. R. Passoni, E. Morandi, and A. Capria, "Functional evaluation of the endotics system, a new disposable self-propelled robotic colonoscope: In vitro tests and clinical trial," *Int. J. Artif. Organs*, vol. 32, no. 8, pp. 517–527, Aug. 2009, doi: 10.1177/039139880903200806.

[25] THD America, Inc. Accessed: May 2, 2023, [Online]. Available: https://www.thdlab.it/

[26] L.L. Lai et al., "Feasibility and safety study of a high resolution wide field-of-view scanning endoscope for circumferential intraluminal intestinal imaging," *Sci. Rep.*, vol. 11, 2021, Art. no. 3544, doi: 10.1038/s41598-021-82962-2.

[27] G. Lule, Ed., *Current Concepts in Colonic Disorders*. London, U.K.: IntechOpen, 2011.

[28] J. Ortega Alcaide et al., "Tether-colon interaction model and tribological characterization for front-wheel driven colonoscopic devices," *Tribol. Int.*, vol. 156, Apr. 2021, Art. no. 106814, doi: 10.1016/J.TRIBOINT.2020.106814.

[29] H. Abidi and M. Cianchetti, "On intrinsic safety of soft robots," *Front. Robot. AI*, vol. 4, p. 6, Feb. 2017, doi: 10.3389/FROBT.2017.00005/BIBTEX.

[30] J. Sosna, J. Bar-Ziv, E. Libson, M. Eligulashvili, and A. Blachar, "CT colonography: Positioning order and intracolonic pressure," *Amer. J. Roentgenol.*, vol. 191, no. 4, 2008, Art. no. 1100, doi: 10.2214/AJR.07.3303.

[31] S. Song et al., "Integrated design and decoupled control of anchoring and drug release for wireless capsule robots," *IEEE/ASME Trans. Mechatronics*, vol. 27, no. 5, pp. 2897–2907, Oct. 2022.

[32] M. Rehan, I. Al-Bahadly, D. G. Thomas, and E. Avci, "Measurement of peristaltic forces exerted by living intestine on robotic capsule," *IEEE/ASME Trans. Mechatron.*, vol. 26, no. 4, pp. 1803–1811, Aug. 2021.

[33] J. Zhang et al., "Learning material parameters and hydrodynamics of soft robotic fish via differentiable simulation," in *Proc. IEEE/RSJ Int. Conf. Intell. Robots Syst.*, 2022, p. 8.

[34] L. Lindenroth, D. Stoyanov, K. Rhode, and H. Liu, "Toward intrinsic force sensing and control in parallel soft robots," *IEEE/ASME Trans. Mechatron.*, vol. 28, no. 1, pp. 80–91, Feb. 2023.

[35] G. A. Formosa, J. M. Prendergast, J. Peng, D. Kirkpatrick, and M. E. Rentschler, "A modular endoscopy simulation apparatus (MESA) for robotic medical device sensing and control validation," *IEEE Robot. Automat. Lett.*, vol. 3, no. 4, pp. 4054–4061, Oct. 2018, doi: 10.1109/LRA.2018.2861015.

[36] M. Finocchiaro et al., "Physical simulator for colonoscopy: A modular design approach and validation," *IEEE Access*, vol. 11, pp. 36945–36960, 2023, doi: 10.1109/ACCESS.2023.3266087.
[37] D. B. Schembre et al., "Spiral overtube–assisted colonoscopy after incomplete colonoscopy in the redundant colon," *Gastrointestinal Endoscopy*, vol. 73, no. 3, pp. 515–519, 2011, doi: 10.1016/j.gie.2010.11.047.
[38] M. T. Wei, S. Friedland, R. R. Watson, and J. H. Hwang, "Use of a rigidizing overtube for altered-anatomy ERCP," *VideoGIE*, vol. 5, no. 12, pp. 664–666, 2020, doi: 10.1016/j.vgie.2020.08.003.

Yu Huan received the M.Sc. degree in biomedical engineering from the University of Dundee, Dundee, U.K., in 2016, and the Ph.D. degree in biorobotics from the Scuola Superiore Sant'Anna, Pisa, Italy, 2020.

His research interests include surgical end effectors, manipulators, and actuators.

Xuyang Ren received the B.Sc. and M.Sc. degrees in mechanical engineering from the Tianjin University, Tianjin, China, in 2016 and 2019, respectively, and the Ph.D. degree in biorobotics from the Scuola Superiore Sant'Anna, Pisa, Italy, in 2023.

His research interests include endoscopic devices, surgical robotics, and soft actuators for medical applications.

Andrea Firrincieli received the M.Sc. degree in aerospace engineering from the University of Pisa, Pisa, Italy, in 2015.

He is collaborator with Healthcare Mechatronics Lab., the BioRobotics Institute, Scuola Superiore Sant'Anna, Pisa, Italy, and collaborator with Mediate Srl, (active in industrial and medical robotics). He has technical expertise in endoscopic devices (two scientific publications, one patent). He is involved in technical and management in national/international projects. His research interests include medical, collaborative and industrial robotics, robotics for recycling, and healthcare mechatronics.

Luigi Manfredi (Member, IEEE) received the M.Sc. degree in computer engineer from the University of Pisa, Pisa, Italy, in 2001.

He is Senior Lecturer (P.I.) and Baxter Fellow with Division of Imaging Science and Technology, School of Medicine, University of Dundee, Dundee, U.K. His research interests focusses on smart endorobots for gastrointestinal tract.

Mr. Manfredi is recipient of Surgical Innovation Award (SAGES Congress 2013, USA) and runner-up prize for the Emerging Technology Award (SAGES Congress 2016, USA). He is a member of the EAES Technology Committee.

Matteo Cianchetti (Member, IEEE) received the M.Sc. degree in biomedical engineering from the University of Pisa, Pisa, Italy, in 2007, and the Ph.D. degree in biorobotics from the Scuola Superiore Sant'Anna, Pisa, Italy, in 2011.

He is an Assistant Professor with Scuola Superiore Sant'Anna (The BioRobotics Institute), Head of Soft Mechatronics for Biorobotics Lab. He has authored or coauthored >100 international papers and reviewer for >10 international journals. He is involved in EU-funded projects on soft robotics. His research interests include bioinspired robotics, soft actuators, smart sensors, and flexible mechanisms.

Dr. Cianchetti is Chair of the IEEE TC on Soft Robotics.

Alberto Arezzo received the specialist certification in general surgery from the University of Genoa, Genoa, Italy and from University of Tuebingen, Tuebingen, Germany, in 1997.

He is an Associate Professor of surgery with the Department of Surgical Sciences, University of Turin, Turin, Italy. He has authored >280 scientific publications and is clinical expert with >5000 interventions. His research interests include diagnosis and treatment of digestive tract disease, with specific interest in minimally invasive therapy.

Edoardo Sinibaldi (Member, IEEE) received the B.Sc. and M.Sc. in aerospace engineering from the University of Pisa, Pisa, Italy, in 2002, and the Ph.D. degree in mathematics for technology and industry from the Scuola Normale Superiore, Pisa, Italy, in 2006.

He was research intern at Rolls-Royce plc, Derby, U.K., and he is researcher with the Italian Institute of Technology. He has authored ∼60 (international) journal papers and ∼20 conferences papers, 7 patents and 1 book, and is also reviewer for ∼70 international journals, besides conferences and research proposals. His research interests include modeling and model-based design (for biomedical applications), soft robotics, magnetics, physical intelligence.

Dr. Sinibaldi is Associate/Academic Editor for Scientific Reports, Frontier in Bioengineering and Biotechnology, PLOS One.

Gastone Ciuti (Senior Member, IEEE) the M.Sc. degree in biomedical engineering from the University of Pisa, Pisa, Italy, in 2008, and the Ph.D. degree in biorobotics from the Scuola Superiore Sant'Anna, Pisa, Italy, in 2012.

He is an Associate Professor of bioengineering with Scuola Superiore Sant'Anna (The BioRobotics Institute), Head of Healthcare Mechatronics Lab. He has authored >110 scientific publications on medical devices/robotics and >15 patents. His research interests include surgical robotics, medical robotics, collaborative robotics, and healthcare mechatronics.

He is Member of the Technical Committee in BioRobotics of IEEE-EMBS, Associate Editor of IEEE JOURNAL OF BIOENGINEERING AND HEALTH INFORMATICS, IEEE TRANSACTIONS ON BIOMEDICAL ENGINEERING, and IEEE TRANSACTIONS ON MEDICAL ROBOTICS AND BIONICS.